# UC Irvine
## UC Irvine Previously Published Works

**Title**

Scattering of light by molecules over a rough surface.

**Permalink**

**Journal**

**ISSN**

**Authors**

Long, Maureen
Khine, Michelle
Kim, Arnold D

**Publication Date**

2010-05-01

**DOI**

**Copyright Information**

Peer reviewed

# Scattering of light by molecules over a rough surface

**Maureen Long,[1] Michelle Khine,[2] and Arnold D. Kim[1],***

[1]*School of Natural Sciences, 5200 North Lake Road, University of California, Merced, Merced, California 95343, USA*
[2]*Department of Biomedical Engineering, University of California, Irvine, Irvine, California 92697-2715, USA*
*\*Corresponding author: adkim@ucmerced.edu*

We present a theory for the multiple scattering of light by obstacles situated over a rough surface. This problem is important for applications in biological and chemical sensors. To keep the formulation of this theory simple, we study scalar waves. This theory requires knowledge of the scattering operator (*t*-matrix) for each of the obstacles as well as the reflection operator for the rough surface. The scattering operator gives the field scattered by the obstacle due to an exciting field incident on the scatterer. The reflection operator gives the field reflected by the rough surface due to an exciting field incident on the rough surface. We apply this general theory for the special case of point scatterers and a slightly rough surface with homogeneous Dirichlet and Neumann boundary conditions. We show examples that demonstrate the utility of this theory. © 2010 Optical Society of America

*OCIS codes:* 290.5825, 290.5880, 290.5850, 290.4210.

## 1. INTRODUCTION

Detection and discernment of nucleic acids, proteins, and other biologically relevant small molecules are of critical diagnostic importance [1]. The ability to identify such with high sensitivity enables accurate pathogen identification for environmental protection, food safety, and early disease diagnosis [2]. It allows also for better and faster response to bio-terrorism threats. Most molecular identification methods currently rely on fluorescence readouts in which fluorophores are coupled to specific biomolecules of interest for detection [3].

As the unique blueprint to every organism, nucleic acid sequences are important molecular signatures. The polymerase chain reaction (PCR) coupled with molecular fluorophore readouts enables rapid nucleic acid sequencing for high-sensitivity molecular identification [4]. However, the PCR is complex, costly, and sensitive to contamination. Moreover, it is limited in its ability to multiplex multiple targets [5].

Abnormal protein levels reflect infections and diseases. The gold standard for protein analysis is the fluorescent based enzyme-linked immunosorbent assay (ELISA), with detection limits typically in the picomolar range [5]. Higher sensitivity enables protein markers of infectious diseases and cancers to be detected earlier, at lower concentrations. Earlier diagnosis enables more effective treatment and therefore potentially higher patient survival rates [1]. Despite their exquisite sensitivity and prevalence in molecular detection, fluorophores have significant drawbacks, including photo-bleaching, broad absorption/emission bands, and dependence on expensive excitation and detection equipment. Moreover, fluorescence based labeling and detection typically requires multiple steps [6].

Label-free approaches are more adaptable to point-of-care diagnostics, in which rapid, low-cost, low-powered, portable, and robust systems are required. This is particularly important for first responders of bio-terrorist threats as well as diagnostics for the developing world. Affinity bio-sensors allow for the real-time analysis of bio-specific interactions without the need for labeling molecules. Various optical methods for label-free bio-molecular detection have been explored. Plasmonics involves manipulating light in the subwavelength regime. Nano-structured free-electron metals can be resonantly excited using visible light to produce surface plasmon oscillations that lead to surface-bound electromagnetic fields; these fields can then be manipulated in various ways to detect bio-molecules [2,7,8]. For example, in surface plasmon resonance sensing, molecular adsorption can be detected through changes in the refractive index.

Surface plasmon excitations which leverage subwavelength field localization can also be used for enhanced fluorescence spectroscopy (metal-enhanced fluorescence) or label-free spectroscopy, such as surface-enhanced Raman spectroscopy (SERS) based on more efficient inelastic scattering of light by a molecule in proximity to nanostructured metals. The SERS provides chemical bond information and is considerably more sensitive (down to single molecule sensitivity) than either refractometric or colormetric assays [9]. While one of the best label-free approaches, the challenge with the SERS lies in the trade-off between reliability (with structures made from surface roughening or colloids) and manufacturability (with structures requiring high cost ion beam or electron beam nano-fabrication approaches) [10,11].

We have recently developed a new, low-cost, and nano-structured metallic substrate which can be readily and ro-

bustly integrated into microfluidic devices [12]. These self-assembled nano-structures are due to the stiffness mismatch between retracting shape memory polymers and a thin film of metal. Because the metal cannot retract, it buckles in a predictable manner with controllable predominant wavelengths. A diagram showing this process appears in Fig. 1. These complex non-periodic structures demonstrate strong and tunable plasmon resonances.

A key step in enabling this new fabrication technology for optical sensors lies in understanding optical signals emanating from molecules situated over nanoscale rough metal surfaces. These signals are inherently complicated due to the multiple scattering from the molecules and the rough metal surface. This problem is challenging because one must take into account accurately all of the interactions between the small obstacle and the rough surface. Scattering by the obstacle and the rough surface constitutes challenging problems by themselves. Our objective here is to develop a multiple scattering theory that takes into account interactions between the obstacle and a rough surface.

There are several studies that address obstacle scattering over flat planar surfaces in a variety of contexts [13–15]. For scattering by an obstacle over a rough surface, there are fewer results. In particular, Chiu and Sarabandi [16] studied the special case in which the obstacle is a dielectric cylinder and the surface is only slightly rough. Using the angular correlation function, Jin and Li [17] described a method to detect a scatter target over a randomly rough surface. Johnson [18] studied this problem numerically by taking into account up to fourth-order interactions between the obstacle and the rough surface. Recently, Guo *et al.* [19] used a parallel implementation of the finite-difference/time-domain method to study this problem.

In this paper, we present a systematic method for studying the multiple scattering due to an obstacle situated over a rough surface. This theory requires knowledge of the scattering properties of the obstacle and the rough surface separately. We combine these two operations in a self-consistent way. This theory is simply an extension to the Foldy–Lax theory for multiple scattering [20–23]. We show explicitly that this theory takes into account infinitely many interactions between an obstacle and the rough surface. Thus, this theory provides a foundation for studying carefully the multiple scattering by obstacles over rough surfaces provided that scattering by the obstacle and the rough surface themselves is sufficiently accurate.

It is important to establish here that we do not consider the rough surface to be a *random* rough surface. Although one may not know the exact spatial properties of the surface for these applications, the surface is fixed. Thus, one may perform several calibration steps, if necessary. In particular, we work under the assumption that we can first measure the light scattered by the rough surface without the presence of the obstacles. Then we can measure the light scattered by the obstacles over the rough surface. For this reason, we do not compute any statistical quantities. One may consider computing statistical quantities using this method to make statements about an ensemble of sensors. However, we do not address this issue here.

The remainder of this paper is as follows. In Section 2, we describe the physical problem. We present the self-consistent multiple scattering theory in Section 3. In Section 4, we consider the special case in which the obstacles are point scatterers and the rough surface is a slightly rough perfect electric conductor. We use that simplified special case to work through some examples explicitly in Section 5. We give the conclusions in Section 6. Appendixes A and B give details of the reflection operator for Dirichlet and Neumann slightly rough surfaces, respectively.

## 2. DESCRIPTION OF THE PROBLEM

We seek to develop a theoretical framework to study the interactions of light scattered by obstacles over a rough surface. To study this problem in a simple setting, we study time-harmonic (monochromatic light), scalar wave propagation, and scattering. In particular, we consider a wave incident on several obstacles situated over a rough surface. A sketch of this problem appears in Fig. 2.

In Fig. 2 the rough surface is given by the function $z = f(x,y)$. We consider time-harmonic wave propagation with time dependence $e^{-i\omega t}$ and circular frequency $\omega$. For this scattering problem, we need to solve the following reduced wave or Helmholtz equation:

$$\nabla^2 u + k^2 u = -k^2 \sum_{m=1}^{M} V_m u, \quad \text{in } z > f(x,y), \qquad (2.1)$$

with $\nabla^2 = \partial_x^2 + \partial_y^2 + \partial_z^2$ denoting the Laplacian. Here, $V_m$ for $m = 1, \ldots, M$ denotes the $M$ scattering "potentials" for each of the $M$ scattering obstacles situated over the rough surface. To solve Eq. (2.1), we must prescribe boundary conditions. In particular, we study two different boundary
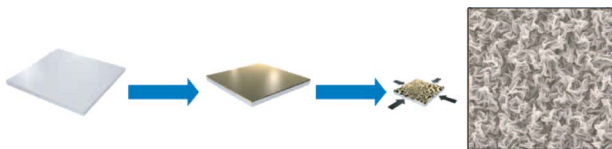


Fig. 1. (Color online) Method for fabricating low-cost and nano-structured metallic substrates reported in [12]. A shape memory polymer is coated with a thin film of metal. Upon heating, the polymer retracts, but the metal does not lead to a buckling of the metal surface. The final image on the right shows a scanning electron micrograph of one such nano-structured metallic substrate fabricated using this method.
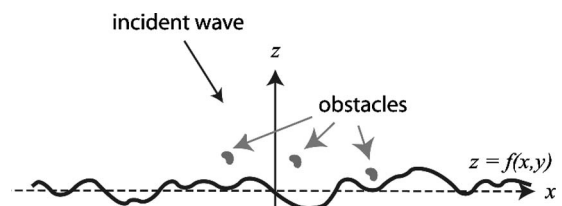


Fig. 2. A sketch of the physical problem. A wave is incident on several obstacles situated over a rough surface. The rough surface is given by the function $z = f(x,y)$. Light scatters from the obstacles and the rough surface.

conditions: Dirichlet and Neumann. The Dirichlet boundary condition is given by

$$u = 0 \quad \text{on } z = f(x,y), \tag{2.2}$$

and the Neumann boundary condition is given by

$$\nu \cdot \nabla u = 0 \quad \text{on } z = f(x,y), \tag{2.3}$$

with

$$\nu = \frac{(\partial_x f, \partial_y f, -1)}{\sqrt{(\partial_x f)^2 + (\partial_y f)^2 + 1}} \tag{2.4}$$

denoting the unit normal to the rough surface.

We write the solution of Eq. (2.1) subject to Eq. (2.2) or Eq. (2.3) as the sum of the incident and scattered fields: $u = u_i + u_s$. The incident field $u_i$ is an incoming solution of homogeneous problem,

$$\nabla^2 u + k^2 u = 0, \tag{2.5}$$

near the bounding surface $z = f(x,y)$. We assume that $u_i$ is known explicitly. The scattered field $u_s$ is an outgoing solution of Eq. (2.1) and is to be found. For this scattered field, we prescribe also Sommerfeld radiation conditions far away from the boundary surface and scattering obstacles.

## 3. SELF-CONSISTENT MULTIPLE SCATTERING THEORY FOR OBSTACLES OVER A ROUGH SURFACE

In what follows, we develop a self-consistent theory for the multiple scattering of light by $M$ obstacles situated over a rough surface. This theory requires knowledge of the scattering operator or the $t$-matrix for each of the obstacles and the reflection operator for the rough surface. Once those operators are established, we combine them in a self-consistent manner to obtain a multiple scattering theory.

The scattering operator $S_m$ gives the field scattered by the $m$th obstacle due to an exciting field. When $S_m$ is known, the scattered field produced by the field $u^E$ exciting the obstacle is given by $S_m u^E$. The scattering operator $S_m$ (otherwise known as the $t$-matrix or transition operator) with kernel $t_m(\mathbf{r}, \mathbf{r}')$ for the $m$th obstacle is given by

$$S_m u^E(\mathbf{r}) = \int_{\chi_m} t_m(\mathbf{r}, \mathbf{r}') u^E(\mathbf{r}') \mathrm{d}\mathbf{r}'. \tag{3.1}$$

Here, $\chi_m$ corresponds to the support of the $m$th obstacle.

The reflection operator $R$ gives the field reflected by the rough surface due to an exciting field. When $R$ is known, the reflected field produced by the field $u^E$ exciting the rough surface is given by $Ru^E$. In general, $R$ is defined by the solution of a surface integral equation derived from the Kirchhoff theory [22–24]. For the special case of a slightly rough surface, we obtain an asymptotic result for $R$ which we will use later.

For the problem corresponding to $M$ obstacles situated over a rough surface, we represent the total field as the following sum:

$$u = u_i + \sum_{m=1}^{M} S_m \phi_m + R \psi. \tag{3.2}$$

Here, $\phi_m$ denotes the field exciting the $m$th obstacle and $\psi$ represents the field exciting the rough surface. These fields are to be determined. Once we have determined them, we can compute $u(\mathbf{r})$ through the evaluation of Eq. (3.2).

We represent the exciting fields as

$$\phi_m = u_i + \sum_{\substack{n=1 \\ n \neq m}}^{M} S_n \phi_n + R \psi \quad \text{in } \chi_m, \quad m = 1, \dots, M, \tag{3.3}$$

$$\psi = u_i + \sum_{m=1}^{M} S_m \phi_m \quad \text{on } z = f(x,y). \tag{3.4}$$

Equations (3.3) and (3.4) comprise a self-consistent system for the exciting fields $\phi_m$ and $\psi$. This self-consistent system is an extension of the so-called Foldy–Lax theory for multiple scattering [20–23]. This extension incorporates scattering by the rough surface. In the same way that the Foldy–Lax theory includes infinitely many interactions, Eqs. (3.3) and (3.4) include infinitely many interactions between the obstacles and the rough surface.

Through substituting Eq. (3.4) into Eq. (3.3), we can construct an $M \times M$ system of equations for exciting fields at the obstacles: $\phi_m$ for $m = 1, \dots, M$. When those exciting fields are known, we compute $\psi$ through the evaluation of Eq. (3.4). In what follows, we will show this computation explicitly for the special case of point obstacles over a slightly rough surface.

## 4. POINT OBSTACLES OVER A SLIGHTLY ROUGH SURFACE

We specialize the general theory given in the previous section to point obstacles situated over a slightly rough surface. For this specific case, the problem reduces to a linear system of algebraic equations. Nonetheless, these simplifications lead to a model problem that allows us to study the complicated interactions between the obstacles and the rough surface.

We say an obstacle, with a characteristic length scale $a$, is small when $ka \ll 1$. For that case, we may use the point scatterer approximation [25] in which the scattering operator for a point obstacle at position $\mathbf{r}_m$ is given by

$$S_m u_i(\mathbf{r}) = \sigma_m G_0(\mathbf{r}; \mathbf{r}_m) u_i(\mathbf{r}_m), \tag{4.1}$$

with $\sigma_m$ denoting the scattering cross-section for the point obstacle and

$$G_0(\mathbf{r}; \mathbf{r}_m) = \frac{e^{ik|\mathbf{r}-\mathbf{r}_m|} - e^{-|\mathbf{r}-\mathbf{r}_m|/a}}{4\pi[1 + (ka)^2]|\mathbf{r} - \mathbf{r}_m|} \tag{4.2}$$

is the free-space Green's function regularized to remove the singularity at $\mathbf{r} = \mathbf{r}_m$ [25]. For $M$ point obstacles at positions $\mathbf{r}_m$ with scattering cross-sections $\sigma_m$ for $m = 1, \dots, M$, Eq. (3.3) reduces to

$$\phi_m = u_i(\mathbf{r}_m) + \sum_{\substack{n=1 \\ n \neq m}}^{M} \sigma_n G_0(\mathbf{r}_m;\mathbf{r}_n)\phi_n + R\psi(\mathbf{r}_m), \quad m = 1, \dots, M.$$

$$(4.3)$$

Furthermore, Eq. (3.4) reduces to

$$\psi(\mathbf{r}) = u_i(\mathbf{r}) + \sum_{m=1}^{M} \sigma_m G_0(\mathbf{r};\mathbf{r}_m)\phi_m \quad \text{on } z = f(x,y).$$

$$(4.4)$$

The exciting fields $\phi_m$ for the point obstacles are just complex scalars.

We now consider the case in which the roughness of the surface $z = f(x,y)$ is small compared to the wavelength. Moreover, we assume that the gradient of the rough surface is small compared to the wavelength. To make this assumption explicit, we introduce the small dimensionless parameter $0 < \epsilon \ll 1$ so that the rough surface is given by $z = \epsilon f(x,y)$. We call this rough surface a "slightly" rough surface. We assume that the function $f(x,y)$ and the parameter $\epsilon$ are known.

In the limit as $\epsilon \to 0^+$, we can compute an asymptotic approximation of the reflection operator $R$ as a perturbation expansion [26,27]. We consider an incident field of the form

$$u_i(x,y,z) = \int \int A(\xi,\eta)e^{i\xi x + i\eta y - i\kappa z}\mathrm{d}\xi\mathrm{d}\eta, \quad (4.5)$$

with $A$ denoting the angular spectrum of the incident field and

$$\kappa = \kappa(\xi,\eta) = \begin{cases} \sqrt{k^2 - \xi^2 - \eta^2}, & \xi^2 + \eta^2 \leq k^2 \\ i\sqrt{\xi^2 + \eta^2 - k^2}, & \xi^2 + \eta^2 > k^2 \end{cases}. \quad (4.6)$$

The field reflected by the slightly rough surface, $Ru_i$ can then be represented as

$$Ru_i(x,y,z) = \int \int \mathcal{R}A(\xi,\eta)e^{i\xi x + i\eta y + i\kappa z}\mathrm{d}\xi\mathrm{d}\eta, \quad (4.7)$$

with $\mathcal{R}$ denoting a linear operator that takes into account scattering due to the surface roughness. In Appendix A, we derive an asymptotic approximation for $\mathcal{R}_D$, the operator for the Dirichlet problem. In Appendix B, we derive an asymptotic approximation for $\mathcal{R}_N$, the operator for the Neumann problem. In what follows, we proceed as if $\mathcal{R}$ is known explicitly.

Evaluating Eq. (4.4) at $z = 0$, we find that

$$\psi(x,y,0) = u_i(x,y,0) + \sum_{m=1}^{M} \sigma_m G_0(x,y,0;\mathbf{r}_m)\phi_m. \quad (4.8)$$

Fourier transforming this result with respect to $x$ and $y$, we obtain

$$\Psi(\xi,\eta) = A(\xi,\eta) + \sum_{m=1}^{M} \sigma_m \hat{g}_0(\xi,\eta;\mathbf{r}_m)\phi_m, \quad (4.9)$$

with $A(\xi,\eta)$ defined in Eq. (4.5),

$$\Psi(\xi,\eta) = \frac{1}{(2\pi)^2} \int \int \psi(x,y,0)e^{-i\xi x - i\eta y}\mathrm{d}x\mathrm{d}y, \quad (4.10)$$

$$\hat{g}_0(\xi,\eta;\mathbf{r}_m) = \frac{i}{8\pi^2\kappa}e^{-i\xi x_m - i\eta y_m + i\kappa|z_m|}. \quad (4.11)$$

In Eq. (4.9), we have made use of the Weyl representation for $G_0$ given by

$$G_0(\mathbf{r};\mathbf{r}') = \frac{1}{(2\pi)^2} \int \int \frac{i}{2\kappa}\exp[i\xi(x - x')$$
$$+ i\eta(y - y') + i\kappa|z - z'|]\mathrm{d}\xi\mathrm{d}\eta. \quad (4.12)$$

Equations (4.11) and (4.12) correspond to the free-space Green's function rather than Eq. (4.2) since we are not evaluating them near the singularity. Now, we introduce the quantities

$$RG_0(\mathbf{r};\mathbf{r}_n) = \int \int \mathcal{R}\hat{g}_0(\xi,\eta;\mathbf{r}_n)e^{i\xi x + i\eta y + i\kappa z}\mathrm{d}\xi\mathrm{d}\eta,$$

$$(4.13)$$

$$Ru_i(\mathbf{r}) = \int \int \mathcal{R}A(\xi,\eta)e^{i\xi x + i\eta y + i\kappa z}\mathrm{d}\xi\mathrm{d}\eta. \quad (4.14)$$

Notice that $RG_0(\mathbf{r};\mathbf{r}_n)$ is the field reflected by the slightly rough surface due to a point source at position $\mathbf{r}_n$. Similarly, $Ru_i(\mathbf{r})$ is the incident field reflected by the slightly rough surface evaluated at position $\mathbf{r}$.

By applying the reflection operator to Eq. (4.8) and evaluating that result at position $\mathbf{r}_m$, we obtain

$$R\psi(\mathbf{r}_m) = Ru_i(\mathbf{r}_m) + \sum_{n=1}^{M} \sigma_n RG_0(\mathbf{r}_m;\mathbf{r}_n)\phi_n. \quad (4.15)$$

Thus, substituting Eq. (4.15) into Eq. (4.3) and rearranging terms yields the following $M \times M$ linear system:

$$\sum_{n=1}^{M} A_{mn}\phi_n = u_i(\mathbf{r}_m) + Ru_i(\mathbf{r}_m), \quad m = 1, \dots, M,$$

$$(4.16)$$

with

$$A_{mn} = \begin{cases} 1 - \sigma_m RG_0(\mathbf{r}_m;\mathbf{r}_m), & m = n \\ -\sigma_n[G_0(\mathbf{r}_m;\mathbf{r}_n) + RG_0(\mathbf{r}_m;\mathbf{r}_n)], & m \neq n. \end{cases}$$

$$(4.17)$$

Upon the solution of Eq. (4.16), we obtain the $M$ complex numbers $\phi_1, \phi_2, \dots, \phi_M$. With those complex numbers known, we can compute $\psi$ through the evaluation of Eq. (4.4). Thus, the field scattered by the point obstacles and the slightly rough surface is given by

$$u_s(\mathbf{r}) = Ru_i(\mathbf{r}) + \sum_{m=1}^{M} \sigma_m[G_0(\mathbf{r};\mathbf{r}_m) + RG_0(\mathbf{r};\mathbf{r}_m)]\phi_m.$$

$$(4.18)$$

To summarize the results of this section, we give the following procedure to compute the field scattered by $M$ point obstacles situated over a slightly rough surface.

1. Prescribe the slightly rough surface $z = \epsilon f(x,y)$.

2. With that slightly rough surface, compute the asymptotic approximation to $\mathcal{R}$ using Eq. (A12) for a Dirichlet surface (Appendix A) or Eq. (B13) for a Neumann surface (Appendix B).

3. Set the positions $\mathbf{r}_m$ and scattering cross-sections $\sigma_m$ for the $M$ point obstacles.

4. Solve Eq. (4.16) to obtain $\phi_1, \phi_2, \ldots, \phi_M$.

5. Evaluate Eq. (4.18) to obtain $u_s(\mathbf{r})$.

## 5. EXAMPLES

In what follows, we consider two particular examples. The first one is for a single point obstacle situated over a slightly rough surface. The second one is for two point obstacles situated over a slightly rough surface. These two examples are relevant for applications of optical sensors for point-of-care diagnostics. The ability to detect extremely low concentrations of analytes in a solution is important for this application, but remains a persistent challenge. For example, the limit of detection for the ELISA, the gold standard, is typically in the picomolar range. To be able to detect molecules at much more dilute concentrations would enable earlier stage detection with a less invasive sampling. Thus, we assume only a few obstacles in a site specific region to test the ability to detect extremely low concentrations.

For both of these examples, we are able to obtain analytical results that we interpret physically. Using those analytical results, we compute asymptotic results for the scattered field $u_s(\mathbf{r})$ evaluated in the far-field.

### A. One Point Obstacle

When there is only one point obstacle with scattering cross-section $\sigma_1$ situated over a slightly rough surface at position $\mathbf{r}_1$, Eq. (4.15) reduces to

$$[1 - \sigma_1 R G_0(\mathbf{r}_1;\mathbf{r}_1)]\phi_1 = u_i(\mathbf{r}_1) + R u_i(\mathbf{r}_1). \quad (5.1)$$

The solution is given by

$$\phi_1 = \frac{u_i(\mathbf{r}_1) + R u_i(\mathbf{r}_1)}{1 - \sigma_1 R G_0(\mathbf{r}_1;\mathbf{r}_1)}. \quad (5.2)$$

Expanding Eq. (5.2) formally, we find that

$$\phi_1 = \sum_{n=0}^{\infty} [\sigma_1 R G_0(\mathbf{r}_1;\mathbf{r}_1)]^n [u_i(\mathbf{r}_1) + R u_i(\mathbf{r}_1)]. \quad (5.3)$$

We can interpret this result in the following way. The first term corresponds to the incident field $u_i$ and the incident field reflected by the slightly rough surface, $R u_i$, exciting the point obstacle. The next term corresponds to the scattering of that exciting field down to the slightly rough surface and reflected back up to excite the point scatterer, and so on. A diagram showing these interactions appears in Fig. 3. Thus, Eq. (5.3) shows that this theory takes into account infinitely many interactions between the point obstacle and the slightly rough surface.

Now that $\phi_1$ is known explicitly, we compute the scattered field through the evaluation of
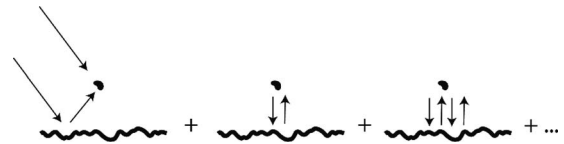


Fig. 3. A diagram showing the interactions between the point obstacle and the slightly rough surface given by Eq. (5.3). In the first diagram, the incident field and the incident field reflected by the rough surface excite the point obstacle. Next, that exciting field is scattered by the point obstacle and reflected by the rough surface to excite the point obstacle again. This series continues to include infinitely many interactions between the point obstacle and the slightly rough surface.

$$u_s(\mathbf{r}) = R u_i(\mathbf{r}) + \sigma_1 [G_0(\mathbf{r};\mathbf{r}_1) + R G_0(\mathbf{r};\mathbf{r}_1)]\phi_1. \quad (5.4)$$

We have computed numerically the results given by Eq. (5.4). All quantities that are given below are in units of the wavelength $\lambda$. For these numerical calculations, we consider a uni-axial slightly rough surface of the form $z = \epsilon f(x)$ with $\epsilon = 0.05$. For this example, we generated one realization of a Gaussian correlated random rough surface with a correlation length of 1.5 and a RMS height of 1 [23]. The point obstacle has scattering cross-section set to $\sigma_1 = 1$. It is located at position $\mathbf{r}_1 = (11.7, 0.0, 0.1)$. The location of the point obstacle in relation to this rough surface is shown in Fig. 4.

A plane wave propagating in the $xz$-plane of the form $u_i = \exp(-ikz)$ is incident on the point obstacle and rough surface. With these considerations, the symmetry with respect to the $xz$-plane is broken only due to scattering by the point obstacle. To compute these fields, we replaced the Fourier transforms in the results from the previous section with the discrete Fourier transforms computed on a $512 \times 512$ grid of the computational domain: $[-25.6, 25.6] \times [-25.6, 25.6]$. Figure 5 shows contour plots of the image $I(x,y)$ defined as

$$I(x,y) = |u_s(x,y,z_0)|^2 - |R u_i(x,y,z_0)|^2 \quad (5.5)$$

for both the Dirichlet (top) and Neumann (bottom) cases. Here, the plane $z_0 = 5.0$ corresponds to the plane on which the light is detected. This difference image $I(x,y)$ corresponds to the subtraction of the direct image without the point obstacles taken at the detector plane from the direct image with the point obstacles taken at the detector
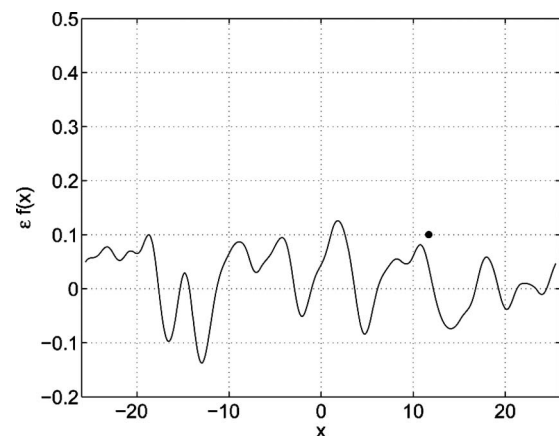


Fig. 4. A plot of the rough surface and point obstacle shown on the $y = 0$ plane. The point obstacle is located at position $\mathbf{r}_1 = (11.7, 0.0, 0.1)$ in units of wavelengths.
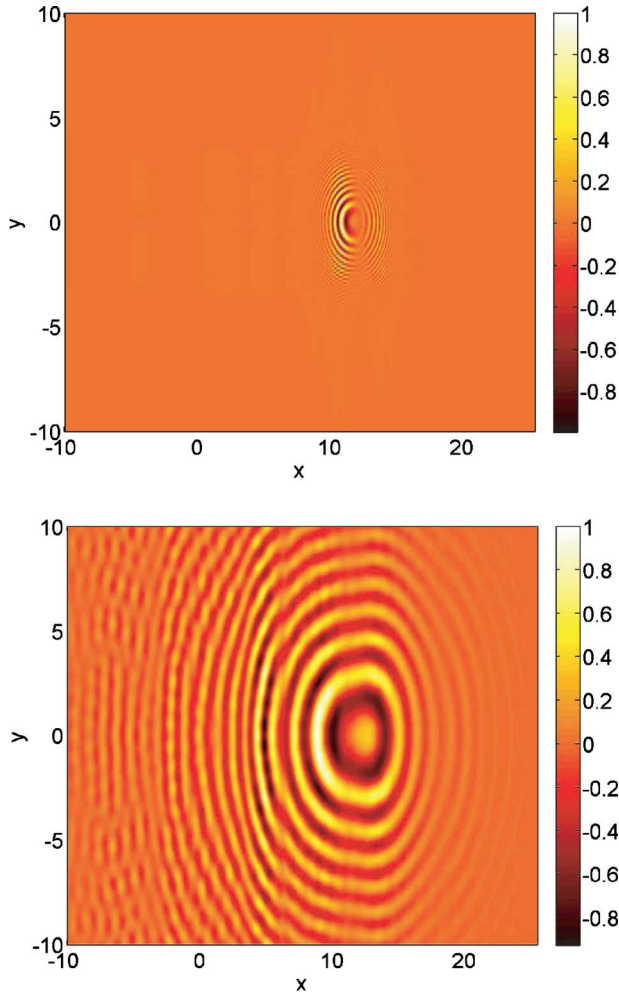
Fig. 5. (Color online) Contour plots of the image $I(x,y)$ defined in Eq. (5.5) corresponding to a single point obstacle shown in Fig. 4 for the Dirichlet (top) and Neumann (bottom) cases.

plane. It is normalized to the maximum absolute value of $I(x,y)$. This difference image shows the complicated interactions between the rough surface and the point obstacle. In Fig. 5, we see distortions of the scattering by the point obstacle by the uni-axial rough surface as faint vertical bands. The Dirichlet surface produces a more localized image about the point obstacle than does the Neumann surface. However, we have observed widely varying results depending on the location of the point obstacle to the rough surface.

Using the standard expression for the far-field Green's function and the method of stationary phase [28], we find that

$$u_s \sim F_1(\hat{\mathbf{s}}) \frac{e^{ikR}}{R}, \quad kR \to \infty, \tag{5.6}$$

with

$$F_1(\hat{\mathbf{s}}) = -i2\pi k s_z \mathcal{R} A(k s_x, k s_y)$$
$$+ \sigma_1 \phi_1 \left[ \frac{e^{-ik\hat{\mathbf{s}} \cdot \mathbf{r}_1}}{4\pi} - i2\pi k s_z \mathcal{R} \hat{g}_0(k s_x, k s_y; \mathbf{r}_1) \right]. \tag{5.7}$$

Here, $\hat{\mathbf{s}} = (s_x, s_y, s_z) = (\sin\theta\cos\varphi, \sin\theta\sin\varphi, \cos\theta)$, with $\theta$

denoting the polar angle and $\varphi$ denoting the azimuthal angle.

### B. Two Point Obstacles
When there are two point obstacles with scattering cross-sections $\sigma_1$ and $\sigma_2$ situated over a slightly rough surface at positions $\mathbf{r}_1$ and $\mathbf{r}_2$, respectively, Eq. (4.15) reduces to

$$\begin{bmatrix} A_{11} & A_{12} \\ A_{21} & A_{22} \end{bmatrix} \begin{bmatrix} \phi_1 \\ \phi_2 \end{bmatrix} = \begin{bmatrix} b_1 \\ b_2 \end{bmatrix}, \tag{5.8}$$

with $A_{mn}$ defined in Eq. (4.16) and

$$\begin{bmatrix} b_1 \\ b_2 \end{bmatrix} = \begin{bmatrix} u_i(\mathbf{r}_1) + R u_i(\mathbf{r}_1) \\ u_i(\mathbf{r}_2) + R u_i(\mathbf{r}_2) \end{bmatrix}. \tag{5.9}$$

This linear system is solved easily and we find that

$$\phi_1 = \frac{1}{\det(A)} \{ [1 - \sigma_2 R G_0(\mathbf{r}_2; \mathbf{r}_2)] b_1 - \sigma_2 [G_0(\mathbf{r}_1; \mathbf{r}_2)$$
$$+ R G_0(\mathbf{r}_1; \mathbf{r}_2)] b_2 \}, \tag{5.10}$$

$$\phi_2 = \frac{1}{\det(A)} \{ [1 - \sigma_1 R G_0(\mathbf{r}_1; \mathbf{r}_1)] b_2 - \sigma_1 [G_0(\mathbf{r}_2; \mathbf{r}_1)$$
$$+ R G_0(\mathbf{r}_2; \mathbf{r}_1)] b_1 \}, \tag{5.11}$$

with

$$\det(A) = 1 - \sigma_1 R G_0(\mathbf{r}_1; \mathbf{r}_1) - \sigma_2 R G_0(\mathbf{r}_2; \mathbf{r}_2)$$
$$- \sigma_1 \sigma_2 [G_0(\mathbf{r}_1; \mathbf{r}_1) G_0(\mathbf{r}_2; \mathbf{r}_2) + G_0(\mathbf{r}_1; \mathbf{r}_1) R G_0(\mathbf{r}_2; \mathbf{r}_2)$$
$$+ R G_0(\mathbf{r}_1; \mathbf{r}_1) G_0(\mathbf{r}_2; \mathbf{r}_2)]. \tag{5.12}$$

Now that $\phi_1$ and $\phi_2$ are known explicitly, we compute the scattered field $u_s(\mathbf{r})$ through the evaluation of

$$u_s(\mathbf{r}) = R u_i(\mathbf{r}) + \sigma_1 [G_0(\mathbf{r}; \mathbf{r}_1) + R G_0(\mathbf{r}; \mathbf{r}_1)] \phi_1 + \sigma_2 [G_0(\mathbf{r}; \mathbf{r}_2)$$
$$+ R G_0(\mathbf{r}; \mathbf{r}_2)] \phi_2. \tag{5.13}$$

We have computed numerically the results given by Eq. (5.13). We use the same rough surface that we used for the numerical example above. The two point obstacles have scattering cross-section set to $\sigma_1 = \sigma_2 = 1$. One of the point obstacles is located at position $\mathbf{r}_1 = (11.7, 0.0, 0.1)$. The other point obstacle is located at position $\mathbf{r}_2 = (9.7, 0.0, 0.1)$. Thus, the two point obstacles are two wavelengths apart from one another. The location of the two point obstacles in relation to this rough surface is shown in Fig. 6.

In Fig. 7 we plot the image $I(x,y)$ defined in Eq. (5.5) for both the Dirichlet (top) and Neumann (bottom) cases. Just as with Fig. 5, the detector plane is $z_0 = 5.0$. These results are similar qualitatively to those in Fig. 5. However, one can observe a distorted dipole pattern resulting from the scattering by the two point obstacles.

Just as we have done for the one point obstacle, we can evaluate $u_s(\mathbf{r})$ in the far-field limit. In doing so, we find that

$$u_s \sim F_2(\hat{\mathbf{s}}) \frac{e^{ikR}}{R}, \quad kR \to \infty, \tag{5.14}$$
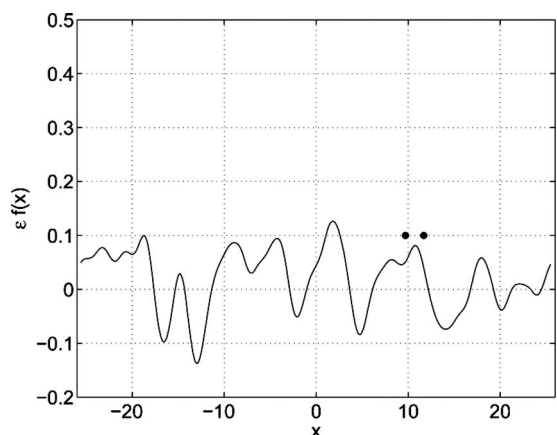
with

Fig. 6.   A plot of the rough surface and two point obstacles shown on the $y=0$ plane. The point obstacles are located at positions $\mathbf{r}_1 = (11.7, 0.0, 0.1)$ and $\mathbf{r}_2 = (9.7, 0.0, 0.1)$ in units of wavelengths.
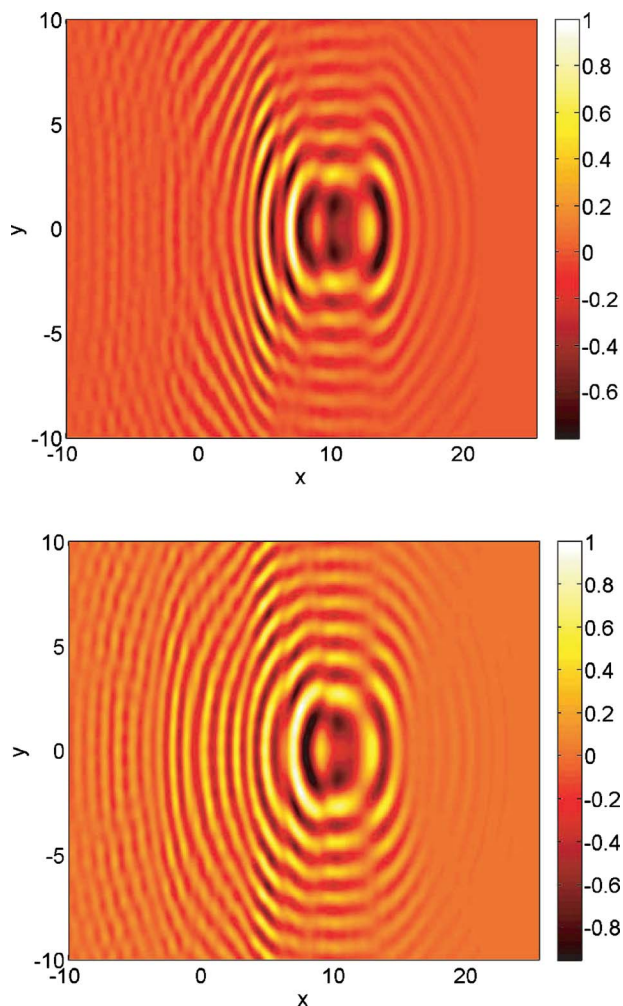




Fig. 7.   (Color online) Contour plots of the image $I(x,y)$ defined in Eq. (5.5) corresponding to two point obstacles shown in Fig. 6 for the Dirichlet (top) and Neumann (bottom) cases.

$$
F_2(\hat{\mathbf{s}}) = -i2\pi ks_z \mathcal{R}A(ks_x, ks_y)
$$

$$
+ \sigma_1 \phi_1 \left[ \frac{e^{ik\hat{\mathbf{s}} \cdot \mathbf{r}_1}}{4\pi} - i2\pi ks_z \mathcal{R}\hat{g}_0(ks_x, ks_y; \mathbf{r}_1) \right]
$$

$$
+ \sigma_2 \phi_2 \left[ \frac{e^{ik\hat{\mathbf{s}} \cdot \mathbf{r}_2}}{4\pi} - i2\pi ks_z \mathcal{R}\hat{g}_0(ks_x, ks_y; \mathbf{r}_2) \right].
$$

$$(5.15)$$

## 6. CONCLUSIONS

We have developed a theoretical framework to study obstacle scattering over a rough surface. This theory involves combining each of the scattering operators for each of the obstacles and the reflection operator for the rough surface in a self-consistent way. For the simple case of point obstacles over a slightly rough Dirichlet or Neumann surface, we are able to obtain analytical results. We have shown analytical and numerical results for the cases involving one and two point obstacles.

This theoretical framework provides, to our knowledge, a critical first step in studying the multiple scattering of light by nano-structured metallic substrates for sensor applications. It takes into account the interactions made between a single molecule and a rough surface. Here, we have addressed this problem in an idealized setting. The obstacles are point scatterers and the rough surface is a small perturbation from a plane. Moreover, the surface is assumed to be a perfect electric conductor.

There remain several theoretical challenges to realize the potential of using nano-structured metallic surfaces for chemical and biological sensors. For example, we will need to consider very rough surfaces rather than slightly rough surfaces. Preliminary data taken from the nano-structured metallic substrates indicate very large surface roughnesses. That means that we will need to compute numerically the reflection operator rather than use an analytical approximation. By assuming that the surface is a perfect electric conductor, we ignore surface plasmons in the problem. To harness the full potential of these sensors, we will need to include these surface plasmons. Therefore, we will have to take into account the optical properties of the metallic material more accurately. In addition, a point scatterer model may be insufficient for capturing the scattering properties of single molecules. Thus, we will have to consider more sophisticated scattering operators.

Despite the fact this simple model that we have studied is limited in practice, it provides valuable insight into this problem. Moreover, it gives a simple setting to test and design single molecule detection and characterization algorithms which require solving the associated inverse problem. We will extend this theory to be more practically useful in the ways mentioned above in our future work.

## APPENDIX A: THE DIRICHLET PROBLEM

The Dirichlet boundary value problem for a slightly rough surface is

$$
\nabla^2 u + k^2 u = 0 \quad \text{in } z > \epsilon f(x,y), \tag{A1}
$$

$$u = 0 \quad \text{on} \ z = \epsilon f(x,y). \tag{A2}$$

We seek the wave field as the sum $u = u_i + Ru_i$, with $u_i$ denoting the wave field incident on the slightly rough surface and $Ru_i$ denoting the wave field scattered by the rough surface. To solve this boundary value problem, we expand $u_i + Ru_i$ in Eq. (A2) in a Taylor series about $z = 0$ and set $z = \epsilon f(x,y)$ to obtain

$$\left[1 + \epsilon f \partial_z + \epsilon^2 \tfrac{1}{2} f^2 \partial_z^2 + \mathcal{O}(\epsilon^3)\right](u_i + Ru_i) = 0 \quad \text{on} \ z = 0. \tag{A3}$$

We derive the asymptotic approximation for the reflection operator $\mathcal{R}_D$ introduced in Eq. (4.7). Here, the $D$ subscript identifies that this operator is for the Dirichlet problem. The incident field $u_i$ is given in Eq. (4.5). We seek the scattered field $Ru_i$ in the form

$$Ru_i(x,y,z) = \int \int B(\xi, \eta) e^{i\xi x + i\eta y + i\kappa z} \mathrm{d}\xi \mathrm{d}\eta, \tag{A4}$$

with $B(\xi, \eta)$ to be found. Substituting Eqs. (4.5) and (A4) into Eq. (A3) and Fourier transforming that result with respect to $x$ and $y$, we find that

$$B(\xi, \eta) = -A(\xi, \eta) + \epsilon i \int \int F(\xi - \xi', \eta - \eta')\kappa(\xi', \eta')[A(\xi', \eta')$$
$$- B(\xi', \eta')]\mathrm{d}\xi'\mathrm{d}\eta' + \epsilon^2 \frac{1}{2} \int \int F(\xi - \xi', \eta - \eta')$$
$$\times \int \int F(\xi' - \xi'', \eta' - \eta'')\kappa^2(\xi'', \eta'')[A(\xi'', \eta'')$$
$$+ B(\xi'', \eta'')]\mathrm{d}\xi''\mathrm{d}\eta''\mathrm{d}\xi'\mathrm{d}\eta'. \tag{A5}$$

Now, we expand $B$ in powers of $\epsilon$ in the form

$$B(\xi, \eta) = B_0(\xi, \eta) + \epsilon B_1(\xi, \eta) + \epsilon^2 B_2(\xi, \eta) + \mathcal{O}(\epsilon^3). \tag{A6}$$

To determine the terms in Eq. (A6), we substitute Eq. (A3) into Eq. (A5) and equate the coefficient of each power of $\epsilon$ to zero. Thus, to $\mathcal{O}(1)$, we obtain

$$B_0(\xi, \eta) = -A(\xi, \eta). \tag{A7}$$

To $\mathcal{O}(\epsilon)$, we obtain

$$B_1(\xi, \eta) = i \int \int F(\xi - \xi', \eta - \eta')\kappa(\xi', \eta')[A(\xi', \eta')$$
$$- B_0(\xi', \eta')]\mathrm{d}\xi'\mathrm{d}\eta' \tag{A8}$$

Substituting Eq. (A7) into Eq. (A8), we find that

$$B_1(\xi, \eta) = i2 \int \int F(\xi - \xi', \eta - \eta')\kappa(\xi', \eta')A(\xi', \eta')\mathrm{d}\xi'\mathrm{d}\eta'$$
$$= i2F * (\kappa A). \tag{A9}$$

To $\mathcal{O}(\epsilon^2)$, we obtain

$$B_2(\xi, \eta) = \frac{1}{2} \int \int F(\xi - \xi', \eta - \eta') \int \int F(\xi' - \xi'', \eta'$$
$$- \eta'')\kappa^2(\xi'', \eta'')[A(\xi'', \eta'') + B_0(\xi'', \eta'')]\mathrm{d}\xi''\mathrm{d}\eta''\mathrm{d}\xi'\mathrm{d}\eta'$$
$$- i \int \int F(\xi - \xi', \eta - \eta')\kappa(\xi', \eta')B_1(\xi', \eta')\mathrm{d}\xi'\mathrm{d}\eta'. \tag{A10}$$

Substituting Eq. (A7) into Eq. (A10), we find that the first term in Eq. (A10) vanishes identically. Thus, we find, after substituting Eq. (A9), that Eq. (A10) becomes

$$B_2(\xi, \eta) = 2 \int \int F(\xi - \xi', \eta - \eta')\kappa(\xi', \eta') \int \int F(\xi' - \xi'', \eta'$$
$$- \eta'')\kappa(\xi'', \eta'')A(\xi'', \eta'')\mathrm{d}\xi''\mathrm{d}\eta''\mathrm{d}\xi'\mathrm{d}\eta'$$
$$= 2F * [\kappa F * (\kappa A)]. \tag{A11}$$

Combining the results, we find that

$$B(\xi, \eta) = \mathcal{R}_D A = -A + \epsilon i2F * \kappa A + \epsilon^2 2F * [\kappa F * (\kappa A)]$$
$$+ \mathcal{O}(\epsilon^3). \tag{A12}$$

## APPENDIX B: THE NEUMANN PROBLEM

The Neumann boundary value problem for a slightly rough surface is given by

$$\nabla^2 u + k^2 u = 0 \quad \text{in} \ z > \epsilon f(x,y), \tag{B1}$$

$$\nu \cdot \nabla u = 0 \quad \text{on} \ z = \epsilon f(x,y). \tag{B2}$$

Just as we have done for the Dirichlet problem in Appendix A, we seek the wave field $u$ as the sum $u = u_i + Ru_i$. To solve this boundary value problem, we expand $u_i + Ru_i$ in Eq. (B2) in a Taylor series about $z = 0$ and set $z = \epsilon f(x,y)$ to obtain

$$- \left[\partial_z + \epsilon(f \partial_z^2 - f_x \partial_x - f_y \partial_y) + \epsilon^2 \left(\tfrac{1}{2} f^2 \partial_z^3 - f f_x \partial_x \partial_z - f f_y \partial_y \partial_z\right)\right.$$
$$\left. + \mathcal{O}(\epsilon^3)\right](u_i + Ru_i) = 0 \quad \text{on} \ z = 0. \tag{B3}$$

We derive an asymptotic approximation for the reflection operator $\mathcal{R}_N$ introduced in Eq. (4.7). Here, the $N$ subscript identifies that this operator is for the Neumann problem. We follow the same procedure that we have done for the Dirichlet problem in Appendix A. By substituting Eqs. (4.5) and (A4) into Eq. (B3) and Fourier transforming that result with respect to $x$ and $y$, we obtain

$$- i\kappa B(\xi, \eta) = - i\kappa A(\xi, \eta) + \epsilon \int \int F(\xi - \xi', \eta - \eta')[\kappa^2(\xi', \eta')$$
$$- (\xi\xi' - \xi'^2) - (\eta\eta' - \eta'^2)][A(\xi', \eta')$$
$$+ B(\xi', \eta')]\mathrm{d}\xi'\mathrm{d}\eta' - \epsilon^2 i \int \int F(\xi - \xi', \eta - \eta')$$
$$\times \int \int F(\xi' - \xi'', \eta' - \eta'')\left[\tfrac{1}{2}\kappa^2(\xi'', \eta'')\right.$$
$$\left. - (\xi'\xi'' - \xi''^2) - (\eta'\eta'' - \eta''^2)\right]\kappa(\xi'', \eta'')[A(\xi'', \eta'')$$

$$- B(\xi'', \eta'')] \mathrm{d}\xi'' \mathrm{d}\eta'' \mathrm{d}\xi' \mathrm{d}\eta'. \tag{B4}$$

We use the same expansion for $B$ given in Eq. (A6). To $\mathcal{O}(1)$, we find that

$$B_0(\xi, \eta) = A(\xi, \eta). \tag{B5}$$

To $\mathcal{O}(\epsilon)$, we find that

$$- i\kappa B_1(\xi, \eta) = \int\int F(\xi - \xi', \eta - \eta')[\kappa^2(\xi', \eta') - (\xi\xi' - \xi'^2)$$
$$- (\eta\eta' - \eta'^2)][A(\xi', \eta') + B_0(\xi', \eta')] \mathrm{d}\xi' \mathrm{d}\eta'. \tag{B6}$$

Substituting Eq. (B5) and making use of the fact that

$$\kappa^2(\xi', \eta') - (\xi\xi' - \xi'^2) - (\eta\eta' - \eta'^2) = k^2 - \xi\xi' - \eta\eta', \tag{B7}$$

we find that Eq. (B6) simplifies to

$$B_1(\xi, \eta) = i2 \int\int F(\xi - \xi', \eta - \eta')\alpha(\xi, \eta; \xi', \eta')A(\xi', \eta') \mathrm{d}\xi' \mathrm{d}\eta'$$
$$= i2 F * (\alpha A), \tag{B8}$$

with

$$\alpha(\xi, \eta; \xi', \eta') = \frac{k^2 - \xi\xi' - \eta\eta'}{\kappa(\xi, \eta)}. \tag{B9}$$

Next, to $\mathcal{O}(\epsilon^2)$ we obtain

$$- i\kappa B_2(\xi, \eta) = i \int\int F(\xi - \xi', \eta - \eta') \int\int F(\xi' - \xi'', \eta' - \eta'')$$
$$\times \left[ \frac{1}{2}\kappa^2(\xi'', \eta'') - (\xi'\xi'' - \xi''^2) \right.$$
$$\left. - (\eta'\eta'' - \eta''^2) \right] \kappa(\xi'', \eta'')[A(\xi'', \eta'')$$
$$- B_0(\xi'', \eta'')] \mathrm{d}\xi'' \mathrm{d}\eta'' \mathrm{d}\xi' \mathrm{d}\eta''$$
$$+ \int\int F(\xi - \xi', \eta - \eta')[\kappa^2(\xi', \eta') - (\xi\xi' - \xi'^2)$$
$$- (\eta\eta' - \eta'^2)]B_1(\xi', \eta') \mathrm{d}\xi' \mathrm{d}\eta'. \tag{B10}$$

Substituting Eqs. (B5) and (B7), we find that Eq. (B6) reduces to

$$B_2(\xi, \eta) = i \int\int F(\xi - \xi', \eta - \eta')\alpha(\xi, \eta; \xi', \eta')B_1(\xi', \eta') \mathrm{d}\xi' \mathrm{d}\eta'. \tag{B11}$$

Substituting Eq. (B8) into Eq. (B11), we find that

$$B_2(\xi, \eta) = - 2 \int\int F(\xi - \xi', \eta - \eta')\alpha(\xi, \eta; \xi', \eta')$$
$$\times \int\int F(\xi' - \xi'', \eta' - \eta'')\alpha(\xi', \eta'; \xi'', \eta'')$$
$$\times A(\xi'', \eta'') \mathrm{d}\xi'' \mathrm{d}\eta'' \mathrm{d}\xi' \mathrm{d}\eta'$$
$$= - 2 F * [\alpha F * (\alpha A)]. \tag{B12}$$

Combining the results, we obtain

$$B(\xi, \eta) = \mathcal{R}_N A = A + \epsilon i2 F * (\alpha A) - \epsilon^2 2 F * [\alpha F * (\alpha A)]$$
$$+ \mathcal{O}(\epsilon^3). \tag{B13}$$

## ACKNOWLEDGMENTS

## REFERENCES

1. C. D. Chin, C. Linder, and S. K. Sia, "Lab-on-a-chip devices for global health: past studies and future opportunities," Lab Chip **7**, 41 (2007).
2. J. Homola, "Present and future of surface plasmon resonance biosensors," Anal. Bioanal. Chem. **377**, 528–539 (2003).
3. S. Weiss, "Fluorescence spectroscopy of single biomolecules," Science **283**, 1676–1683 (1999).
4. T. Sano, C. L. Smith, and C. R. Cantor, "Immuno-PCR: very sensitive antigen detection by means of specific antibody-DNA conjugates," Science **258**, 120 (1992).
5. N. L. Rosi and C. A. Mirkin, "Nanostructures in biodiagnostics," Chem. Rev. (Washington, D.C.) **105**, 1547–1562 (2005).
6. X. Fang, X. Liu, S. Schuster, and W. Tan, "Designing a novel molecular beacon for surface-immobilized DNA hybridization studies," J. Am. Chem. Soc. **121**, 2921 (1999).
7. R. Gordon, D. Sinton, K. L. Kavanagh, and A. G. Brolo, "A new generation of sensors based on extraordinary optical transmission," Acc. Chem. Res. **41**, 1049–1057 (2008).
8. J. Homola, S. S. Yee, and G. Gauglitz, "Surface plasmon resonance sensors: review," Sens. Actuators B **54**, 3–15 (1999).
9. S. Nie and S. R. Emory, "Probing single molecules and single nanoparticles by surface-enhanced Raman scattering," Science **275**, 1102–1106 (1997).
10. G. L. Liu, Y. Lu, J. Kim, J. C. Doll, and L. P. Lee, "Magnetic nanocrescents as controllable surface enhanced Raman scattering nanoprobes for biomolecular imaging," Adv. Mater. **17**, 2683–2688 (2005).
11. P. F. Liao, J. G. Bergman, D. S. Chemla, A. Wokaun, J. Melngailis, A. M. Hawryluk, and N. P. Economou, "Surface-enhanced Raman scattering from microlithographic silver particle surfaces," Chem. Phys. Lett. **82**, 355–359 (1981).
12. C.-C. Fu, A. Grimes, M. Long, C. G. L. Ferri, B. D. Rich, S. Ghosh, S. Ghosh, L. P. Lee, A. Gopinathan, and M. Khine, "Tunable nanowrinkles on shape memory polymer sheets," Adv. Mater. **21**, 4472–4476 (2009).
13. I. V. Lindell, A. H. Sihvola, K. O. Muinonen, and P. W. Baber, "Scattering by a small object close to an interface. I. Exact-image theory formulation," J. Opt. Soc. Am. A **8**, 472–476 (1991).
14. K. O. Muinonen, A. H. Sihvola, I. V. Lindell, and K. A. Lumme, "Scattering by a small object close to an interface. II. Study of backscattering," J. Opt. Soc. Am. A **8**, 477–482 (1991).
15. G. Videen, M. G. Turner, V. J. Iafelice, W. S. Bickel, and W. L. Wolfe, "Scattering from a small sphere near a surface," J. Opt. Soc. Am. A **10**, 118–126 (1993).
16. T. Chiu and K. Sarabandi, "Electromagnetic scattering interaction between a dielectric cylinder and a slightly rough surface," IEEE Trans. Antennas Propag. **47**, 902–913 (1999).
17. Y.-Q. Jin and G. Li, "Detection of a scatter target over a randomly rough surface by using the angular correlation function in a finite-element approach," Waves Random Media **10**, 273–280 (2000).
18. J. T. Johnson, "A numerical study of scattering from an ob-

ject above a rough surface," IEEE Trans. Antennas Propag. **50**, 1361–1367 (2002).

19. L.-X. Guo, J. Li, and H. Zeng, "Bistatic scattering from a three-dimensional object above a two-dimensional randomly rough surface modeled with the parallel FDTD approach," J. Opt. Soc. Am. A **26**, 2383–2392 (2009).
20. L. L. Foldy, "The multiple scattering of waves," Phys. Rev. **67**, 107–119 (1945).
21. M. Lax, "Multiple scattering of waves. II. The effective field in dense systems," Phys. Rev. **85**, 621–629 (1952).
22. L. Tsang and J. A. Kong, *Scattering of Electromagnetic Waves: Advanced Topics* (Wiley, 2001).
23. L. Tsang and J. A. Kong, *Scattering of Electromagnetic Waves: Numerical Simulations* (Wiley, 2001).
24. A. Ishimaru, *Wave Propagation and Scattering in Random Media* (IEEE, 1996).
25. P. de Vries, D. V. van Coevorden, and A. Lagendijk, "Point scatterers for classical waves," Rev. Mod. Phys. **70**, 447–466 (1998).
26. J. G. Watson and J. B. Keller, "Reflection, scattering, and absorption of acoustic waves by rough surfaces," J. Acoust. Soc. Am. **74**, 1887–1894 (1983).
27. A. Ishimaru, J. D. Rockway, and Y. Kuga, "Rough surface Green's function based on the first-order modified perturbation and smoothed diagram methods," Waves Random Media **10**, 17–31 (2000).
28. L. Mandel and E. Wolf, *Optical Coherence and Quantum Optics* (Cambridge U. Press, 1995).